Impact of the Geometrical and Optical Parameters on the Performance of a Cylindrical Remote Phosphor LED
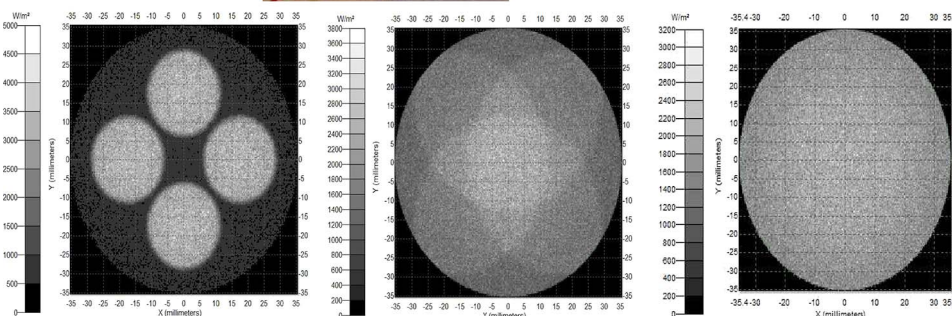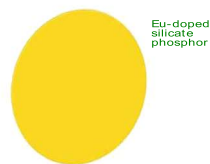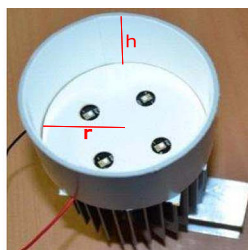
P. C. Acuña
S. Leyre
J. Audenaert
Y. Meuret
G. Deconinck
P. Hanselaer

Impact of the Geometrical and Optical Parameters on the Performance of a Cylindrical Remote Phosphor LED

P. C. Acuña,[1] **S. Leyre,**[1] **J. Audenaert,**[1] **Y. Meuret,**[1]
G. Deconinck,[2] **and P. Hanselaer**[1]

[1]Department of Electrical Engineering (ESAT)/Light and Lighting Laboratory, Technology Campus Ghent, Katholieke Universiteit Leuven, 9000 Ghent, Belgium
[2]Department of Electrical Engineering (ESAT)/Electrical Energy and Computer Architectures (ELECTA), Katholieke Universiteit Leuven, 3000 Leuven, Belgium

Abstract: Remote phosphor light-emitting diode (LED) modules could offer advantages over intimate white phosphor converted LEDs in terms of phosphor operation temperature, light extraction efficiency, and angular color uniformity. Existing commercial devices show a large variety with respect to the dimensions of the mixing cavity, which raises a question about the optimization of the topology. A simplified simulation model applying a two-wavelength approach and considering the remote phosphor as one virtual surface to which three bidirectional scattering distribution functions are attributed (respectively, describing the blue–blue, blue–yellow, and yellow–yellow interactions) is developed and validated. This model has been used to analyze the impact of the cylindrical mixing cavity parameters such as the absolute reflectance, the diffuse-to-specular reflectance ratio, and the height of the mixing cavity, as well as the pitch and angular full-width at half-maximum of the LEDs on the extraction efficiency, the yellow-to-blue ratio, and the irradiance uniformity. It can be concluded that in order to increase the efficacy substantially, the recuperation of the backward emission of the converted light can only be increased by avoiding further interaction with the phosphor plate. To this extent, topologies other than cylindrical mixing cavities must be considered.

Index Terms: Light emitting diodes (LEDs), luminescence and fluorescence, scattering.

1. Background

Light-emitting diodes (LEDs) are commonly used in general lighting applications because of their outstanding characteristics such as high efficacy (lm/W), environmental friendliness, and long lifetime [1]. Two main approaches to create white light with LEDs can be identified: a combination of monochromatic LEDs (commonly red, green, and blue) on the one hand and the combination of monochromatic LEDs with phosphor(s), i.e., phosphor converted LEDs (pc-LEDs), on the other hand. There exists various pc-LEDs topologies: using blue and red LEDs in combination with a green-yellow YAG phosphor [2], [3], using near-UV/blue LEDs with a broad emission spectrum YAG phosphor [4], or using near-UV/blue LEDs alongside a green-yellow YAG phosphor in combination with quantum dots tuned to emit red light [5]. The efficacy of the
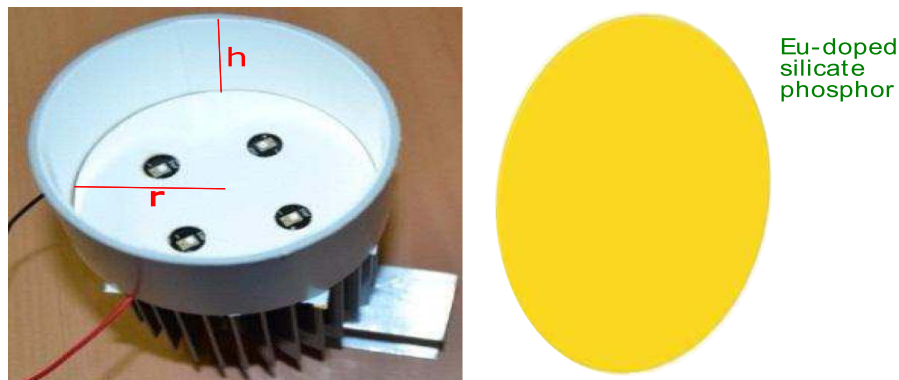
Fig. 1. Test sample of a remote phosphor LED module. (Left) Mixing cavity (radius = 35.4 mm, height = 43 mm). (Right) Remote phosphor converter plate.

monochromatic additive mixing approach is limited by the significantly lower quantum efficiency of green LEDs compared to the near-UV/blue ones (green: < 10%, blue: 35%) [6]. In the pc-LEDs, the power losses originate from the non-ideal external quantum efficiency, the series resistance and the Stokes shift of the phosphor [6]. Regarding the external quantum efficiency, one has to consider the losses in both the chip and the package as a consequence of the absorption in each material, and the reflections due to differences in refractive indices. To minimize the backward scattering of the phosphor toward the chip, the scattered photon extraction method (SPE) was proposed in 2005 [7]. With the SPE, backward scattered light can be recuperated by locating the phosphor at a remote distance from the chip, which increases the probability of back-scattered light to interact with a reflective surrounding. This method promises an enhancement of up to 40% in light extraction efficiency when implemented at package level [7]. Moreover, the remote phosphor technology suppresses angular color variations [8], thus improving the color quality, reduces the glare effect, and makes the LED light engines less sensitive to binning problems and individual LED failures. The remote phosphor concept has been applied not only to the single die package [7], [10]–[12], but also to the chip on board (CoB) package [13] and to LED modules [14]. In the case of a LED module, the mixing cavity efficiency and the re-absorption of recycled converted light by the phosphor become important issues.

Previous reports document the improvement strategies for the light extraction efficiency and color properties of remote phosphor configurations based on the phosphor chemical [15], [16] and physical [17]–[19] properties, but to the best of our knowledge, no research has been done on the impact of the geometrical and optical parameters of the mixing cavity on the user-relevant characteristics of a white remote phosphor LED module. Furthermore, the mixing cavity concepts used in different commercial applications show a rather large variety with respect to its dimensions [20], [21], which raises a question about the optimization of the topology.

The second section describes the device under test which is used to validate the simulation model. The third section describes a simplified ray-tracing simulation model of the remote phosphor LED module. The fourth section presents the validation of the simulation model concerning two aspects: the total light extraction and the spectral distribution. Section 5 presents the main findings from the analysis of the influence of the geometrical and optical parameters of a cylindrical remote phosphor LED module on the performance.

2. Test Device

The mixing cavity (MC) of the experimental remote phosphor LED module under test is chosen to be cylindrical with a radius (r) of 35 mm and a height (h) of 43 mm. The inner surface of the MC is covered with Mylar polyethylene terephthalate (MPET) (see Fig. 1). On the base of the MC, four InGaN blue LEDs are mounted. The exterior surface of the base has been mounted on a heatsink. The remote phosphor converter plate (RPC), consisting of a Eu-doped silicate
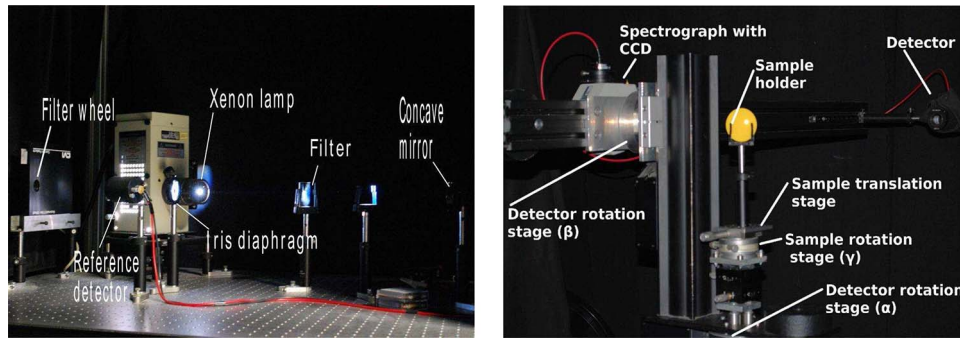
Fig. 2. Bidirectional scattering distribution function measuring setup. (Left) Illumination part. (Right) Detection part.

phosphor film coated onto a diffusing polycarbonate plate, is mounted on top of the MC, with the phosphor film facing the MC.

The four LEDs at the base of the module are introduced in the ray-tracing simulation program using a ray file measured with a near-field goniophotometer (RiGO 801-lamp), equipped with a luminance camera and an illuminance meter on the rotating detection part. The ray file used during the simulation contains 3 million rays; hence, the data array comprises 3 million septuples describing the starting position, the orientation, and the radiant or luminous flux of each ray.

The scattering properties of the MPET are modeled using the bidirectional reflectance distribution function (BRDF). The monochromatic BRDF is defined as the ratio of the differential spectral radiance of the sample at a particular viewing angle to the differential spectral irradiance on the sample from a particular incident angle

$$q_e = \frac{dL_{e,s}(\theta_i, \phi_i, \theta_s, \phi_s)}{dE_{e,i}(\theta_i, \phi_i)} \left[\frac{1}{sr}\right]. \tag{1}$$

The monochromatic BRDF is measured with a custom-made setup [22], which has been specially devised for measuring the bidirectional scattering distribution function (BSDF) in both reflection (BRDF) and transmission (BTDF). The setup consists of two major parts shown in Fig. 2: the illumination part (left) and the detection part (right). The illumination part consists of a Xe-lamp with secondary optics to create a collimated light bundle (diameter of 14 mm). A set of neutral density filters can be inserted in the light path to increase the dynamic range of the measurement setup. Furthermore, an additional filter can be introduced to adjust the spectrum. On the other hand, the detection unit consists of a circular detector aperture with adjustable diameter of maximum 25.4 mm located at a distance of 886 mm from the sample, resulting in a maximum solid angle of 6.25×10^{-4} sr. The detector head, mounted on a bench, is connected with an optical fiber to a spectrometer with a CCD. The detector head can be rotated around the central sample holder with the use of two rotation stages. Furthermore, the setup includes a double beam correction to correct for long term drift of the illumination system. The total measurement uncertainty is approximately 3%.

The BRDF (q_e) of the MPET material used in the mixing cavity illuminated at an angle of incidence of 45 degrees is illustrated in Fig. 3. On the left, the BRDF in the incident plane is illustrated in rectangular coordinates, while on the right, the BRDF for the whole hemisphere is displayed in a polar diagram; the normal of the sample located at the origin. The specular component can be clearly identified and amounts 1.5% of the total reflectance. The total reflectance is 98.5%.

Likewise, both the monochromatic and bi-spectral BSDF describing the three light interactions defined for the remote phosphor plate [23], i.e., blue incident-blue scattered (*bibs*), yellow incident-yellow scattered (*yiys*), and blue incident-yellow scattered (*biys*), were characterized using the same instrument. A complete analysis has been presented in a former paper [23]. BSDF
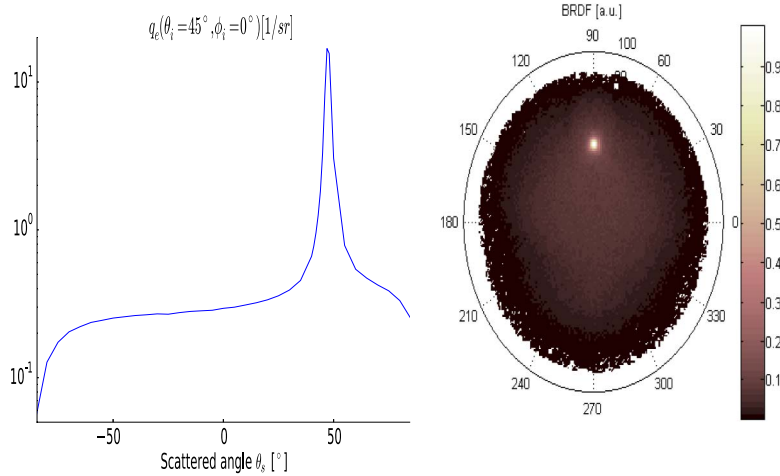
Fig. 3. Bidirectional reflectance distribution function (q_e) of the MPET reflective material when illuminated with a collimated beam at an incident angle of 45°. BRDF in the incident plane in rectangular coordinates (left) and a hemispherical view in polar coordinates (right).
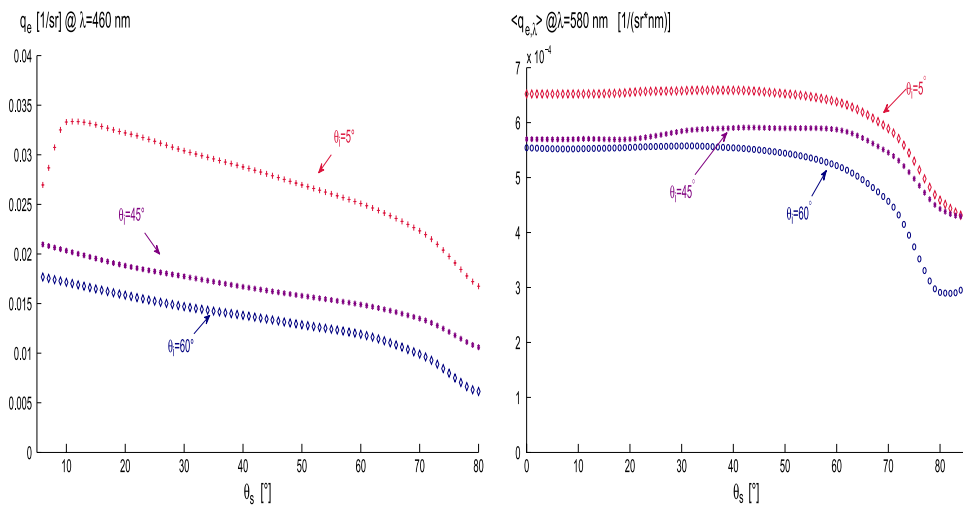

Fig. 4. Monochromatic BTDF for the *bibs* at $\lambda = 460$ nm (left) and averaged bi-spectral BTDF for the *biys* (right) interaction at $\lambda = 580$ nm. The angles of incidence are 5°, 45° and 60°.

results for the interactions *bibs* (q_e @460 nm) and *biys* ($\langle q_{e,\lambda} \rangle$ @580 nm) in the transmission mode are illustrated in Fig. 4 for three incident angles as a function of the scattered angle in the incident plane. The BTDF for the *bibs* interaction is shown for a wavelength of 450 nm, while, the bi-spectral BTDF for the *biys* was averaged over the emission spectrum of the blue LEDs and is presented for 580 nm. As can be observed, the forward scattered blue light is, due to an increased path length and absorption, decreasing with scattering angle, while the converted forward emission is more Lambertian.

3. Ray Tracing Simulation Model

In the current work, all simulations have been performed using the simulation software Trace-Pro, although other simulation packages could be used. The coordinate system used in *Trace-Pro* to represent the BSDF of the MPET is the one defined by Harvey-Shack [24], which differs from both the global coordinate system (measuring setup) and the sample coordinate system. The conversion between coordinate systems is addressed according to the method explained
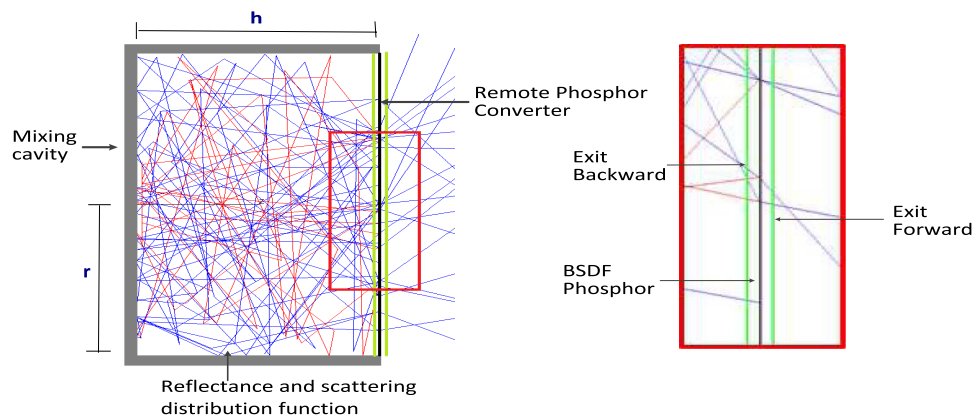
Fig. 5. Geometrical representation of the remote phosphor LED module (left); zoom in of the remote phosphor converter representation and the virtual exit surfaces used in the simulation (right).

by Audenaert in [25]. The BRDF asymmetric table is assigned as a property to both the inner wall and the base of the cylindrical mixing cavity.

The RPC in interaction with short-wavelength light within the excitation spectrum undergoes elastic scattering and wavelength conversion. Attempts to model the phosphor element of a single die LED with intimate YAG phosphor have been reported in [11] and [26]. Liu *et al.* measured the reflected and transmitted flux of the "blue" excitation photons and the "yellow" emitted photons using a double-integrating-sphere. The Kubelka–Munk theory, complemented with the wavelength conversion phenomena, has also been used to predict the backward and forward scattering of a YAG:Ce-based phosphor film as a function of the thickness, phosphor concentration and particle size assuming homogeneous concentration [27] and gradients of concentration across the thickness [28], [29]. In [30], a ray tracing model based on Mie theory using the microscopic parameters of the phosphor and the embedding matrix was defined. These models either do not consider the angular dependence in the scattering process, or require many microscopic parameters, which are hard to acquire. An alternative approach using macroscopic parameters, i.e., scattering coefficient, absorption coefficient and phase function, to model the volume scattering and wavelength conversion in the RPC has been proposed by Leyre *et al.* in [31].

In this paper, the optimization addresses mainly the influence of both the mixing cavity and the pump source parameters on the light extraction ratio (LER) and the yellow-to-blue ratio (YBR) of the remote phosphor LED module. For this reason, the scattering and fluorescent conversion in the RPC are modeled by their experimental accessible BRDF and BTDF characteristics. Hence, the three BSDFs determined for the RPC are implemented as asymmetric tables and sequentially assigned to the geometrical representation. In principle, every single wavelength within the visible range should be traced individually, taking into account the wavelength conversion process, as reported by Leyre *et al.* in [31]. To address the simulation in a simplified way, a two wavelength approximation is adopted where the blue and yellow regions; correspondingly the wavelength ranges [440–470 nm] and [471–740 nm] are considered as one wavelength each.

The simulation starts with importing the measured ray file of the blue LED base. Such a file contains data in photometric units. The LED spectral power distribution is concentrated at 452 nm with a full-width at half-maximum (FWHM) of 20 nm. Following the two-wavelength approach, the luminous flux from the ray file is converted into a single radiometric power value by scaling the relative spectral flux of the blue LED as obtained with a custom-made integrating sphere [32] to the luminous flux. This monochromatic ray file ($\lambda = 452$ nm) along with the geometrical representation of the mixing cavity is traced in order to generate an equivalent ray file of the dummy surface at the exit plane of the mixing cavity just below the RPC (see the left side of Fig. 5). This equivalent ray file interacts with the BRDF and BTDF tables *bibs* and *biys*.

For each of the dummy surfaces "Exit Backward" and "Exit Forward" (see the right side of Fig. 5), two new ray files are created, i.e., one for each wavelength, using the corresponding
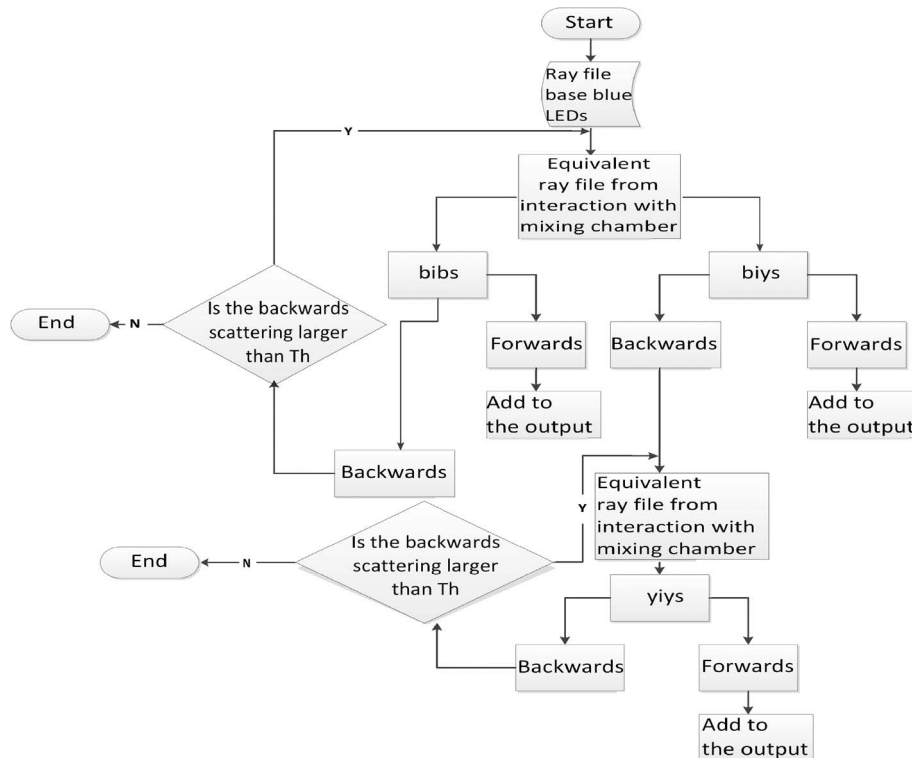
Fig. 6. Simulation algorithm for the light interactions in the remote phosphor LED module. "Th" stands for "threshold."

TABLE 1

Measurement and simulation results of the blue, yellow, and total radiant flux of the remote phosphor LED module

	Blue radiant flux	Yellow radiant flux	Total radiant flux
Simulation	0.058	0.472	0.530
Measurement	0.058	0.491	0.550

BRDF and BTDF table. The incident ray table is saved. The forward ray files for blue and yellow are added to the total output, whereas the interaction of the backward ray files with the mixing cavity is again simulated as long as the integrated power is larger than a defined threshold (Th). If the backward file source is blue, it will follow the previously described procedure, whereas if it is yellow, it will interact with the BSDF table of the *yiys* interaction after being recycled by the mixing cavity. The algorithm that describes the multiple interactions experienced by the light in both the MC and the RPC is schematically illustrated in Fig. 6. The simulation algorithm in Fig. 6 is implemented using the programming language Scheme, which is the default macro programming language integrated with the ray-tracing simulation software *TracePro*.

4. Model Validation

4.1. Total Flux

From the simulations, a forward ray file for both the blue and the yellow equivalent wavelength is calculated by adding the contributions of each simulation step. The total flux for each equivalent wavelength is compared with its experimental counterpart in Table 1, as measured with an integrating sphere.
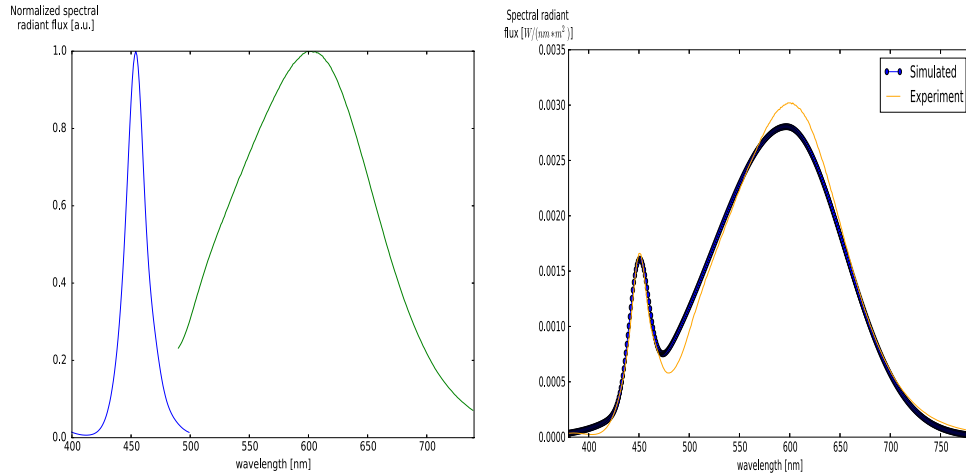
Fig. 7. Spectrum reconstruction from the two wavelength results. (Left) Normalized blue and yellow spectrum. (Right) and simulated spectral radiant power spectra of the module.

The good agreement between the measurements and the simulations is a good indication of the reliability of the simulation model. From the simulations, it is seen that only 53% of the incident radiant power is extracted from the remote phosphor LED module. After the first interaction of the blue beam with the phosphor plate, 31% of the power is scattered forward (5% blue and 26% yellow), whereas 37% is scattered backward (11% blue and 26% yellow). In the recycling process of this backward yellow scattered power, 7% of the total power is lost, which is attributed to the mixing cavity efficiency and the non-fluorescent absorption losses experienced by the recycled yellow contribution travelling through the phosphor plate. More details on the power budget of a RPC can be found in [23]. An ideal mixing cavity would be capable of extracting all the back scattered light.

4.2. Spectral Distribution

From the two-wavelength approach, it is possible to express the radiant flux simulation results given in Table 1 in spectral terms by redistributing the blue and yellow power over the relative spectrum of the blue LEDs and over the emission spectrum of the phosphor plate. The relative normalized spectrum $\Phi_{e,\lambda}^{NORM}(\lambda_i)$ of the blue range (from 380 nm to 500 nm) was measured by positioning the exit aperture of the mixing cavity without the RPC at the detection port of the integrating sphere. The normalized spectrum of the "yellow" range (from 500 nm to 780 nm) is obtained by positioning the phosphor plate at the detection port, while excited by an LED identical to those used in the mixing cavity. These normalized spectra are presented on the left side of Fig. 7. The spectra can be modeled by Gaussian curves [see (2) and (3)], as suggested by Zheng in [33]. For the blue and yellow regions, a Gaussian curve S_{blue} and a modified Gaussian curve S_{yellow} have been selected.

$$S_{blue} = e^{-C\left(\frac{\lambda-\lambda_{p1}}{\Delta\lambda_1}\right)^2} \tag{2}$$

$$S_{yellow} = e^{-C\left(\frac{\lambda-\lambda_{p2}}{\Delta\lambda_2(1+sign(\lambda-\lambda_{p2})\cdot\alpha)}\right)^2}. \tag{3}$$

The curve fitting parameters are summarized in Table 2. A determination coefficient of 0.98 and 0.99 for the blue and yellow spectra has been obtained, respectively.

TABLE 2

Fitting parameters of the curve reproducing the simulated spectrum

Constant	C	$4ln(2)$
Peak wavelength blue	λ_{p1} [nm]	450.1
FWHM blue	$\Delta\lambda_1$ [nm]	22.9
Determination coefficient for blue	[—]	0.98
Peak wavelength yellow	λ_{p2} [nm]	596.7
FWHM yellow	$\Delta\lambda_2$ [nm]	154.3
Asymmetry constant	α	-0.12
Determination coefficient for yellow	[—]	0.99

The absolute spectrum of the remote phosphor module can be considered as a linear combination of the S_{blue} and S_{yellow} curve with only two variables: A_1 and A_2. The variables are calculated by solving the following linear system:

$$\Phi_{e,blue}^{sim} = \sum_{\lambda_i=380}^{500} \left[A_1 S_{blue}(\lambda_i) + A_2 S_{yellow}(\lambda_i)\right]\cdot\Delta\lambda_i = A_1\cdot\sum_{\lambda_i=380}^{500} S_{blue}(\lambda_i)\cdot\Delta\lambda_i + A_2\sum_{\lambda_i=380}^{500} S_{yellow}(\lambda_i)\cdot\Delta\lambda_i$$

$$\Phi_{e,yellow}^{sim} = \sum_{\lambda_i=501}^{780} \left[A_1 S_{blue}(\lambda_i) + A_2 S_{yellow}(\lambda_i)\right]\cdot\Delta\lambda_i = A_1\cdot\sum_{\lambda_i=501}^{780} S_{blue}(\lambda_i)\cdot\Delta\lambda_i + A_2\sum_{\lambda_i=501}^{780} S_{yellow}(\lambda_i)\cdot\Delta\lambda_i$$

with A_1 and A_2 being the gain of both contributions and $\Phi_{e,blue}^{sim}$ and $\Phi_{e,yellow}^{sim}$ the radiant optical power, as determined from the two wavelength simulations (see Table 1). The solution for A_1 and A_2, given by the values 1.22e-3 and 2.80e-3, respectively, are now being used to calculate the resulting radiant flux spectrum which is presented on the right side of Fig. 7.

The simulation results overestimate slightly the optical power near 470 nm and underestimates the yellow emission. For most of the phosphors used to produce white light in combination with near-UV/blue LEDs, the excitation and emission spectrum do overlap [34]. Since a photon inside the material may undergo several scattering and absorption events, a photon can be re-absorbed in the material before escaping the bulk [35]. These multiple events, however, are not considered in the simplified two-wavelength approach and this can explain the deviation between the simulation and experiment.

5. Impact of Geometrical and Optical Parameters

5.1. Input Parameters

The simulation model developed for the remote phosphor module allows for the determination of some user-relevant output parameters, such as the luminous efficacy and the color quality, which in turn depend on the LER and the YBR, respectively. The LER is defined as the ratio of total extracted optical flux from the remote phosphor module to the emitted flux by the pump LEDs and is one of the main parameters determining the final efficiency of the device. The YBR designates the ratio of yellow to blue extracted fluxes from the remote phosphor module, with the radiant flux in the blue and yellow regions corresponding to the integration of the spectral radiant flux between the intervals [380–470 nm] and [471–780 nm], respectively. This parameter gives an indication of the conversion process efficiency, the final color point and the correlated color temperature.

Additionally, when the phosphor plate is excited by a highly non-uniform irradiance distribution, high-dense irradiance spots could induce high temperatures of the RPC that could locally quench the conversion efficiency of the phosphor and degrade the phosphor lifetime, as reported in [9], [33], and [36]. Therefore, the third output parameter which has been considered is the irradiance distribution on the phosphor plate side facing the mixing cavity. This parameter will give information about the mixing capabilities of the cavity.
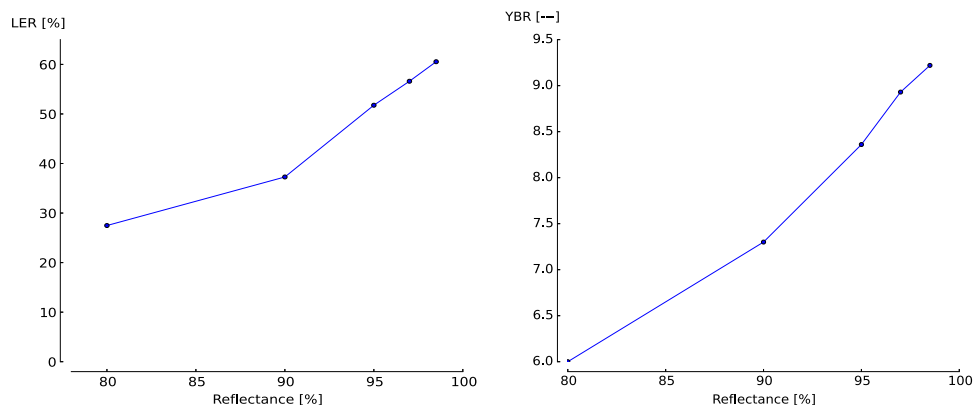
Fig. 8. LER (left) and YBR (right) of the remote phosphor LED module for different total reflectance values of the mixing cavity (height = 43 mm; diffuse-to-specular ratio = 98.5%; LED intensity distribution: Lambertian).

The geometrical and optical input parameters of the pump-LEDs and mixing cavity that will be varied in the simulation are the following:

- total absolute reflectance value of the reflective material;
- diffuse-to-specular ratio of the reflective material;
- height of the mixing cavity;
- intensity distribution of the pump source;
- spatial LED pitch.

From these parameters, the spatial LED pitch did not have any significant influence on the efficiency performance of the remote phosphor module and will not be discussed further. The impact of the other input parameters on the output parameters is described in the following subsections.

5.2. Total Absolute Reflectance and Diffuse-to-Specular Ratio

It may be obvious that the highest possible reflectance of the material used for the mixing cavity will produce the highest extraction efficiency for a certain geometrical configuration. However, as presented in [33], to obtain a subtle increase in the reflectance, the cost may increase significantly. Therefore, the impact of the total absolute reflectance of the mixing cavity on the light engine performance is evaluated by varying its value between 80% and 98%. The results are shown in Fig. 8 and reveal that a decrease of 20% in the total reflectance brings the LER from 58% to 28%. Interestingly, the YBR also decreases from 9 to 6 with the reduction of the reflectance value due to lowering of the recycled yellow light. Hence, changes in the reflectance will also influence the color correlated temperature (CCT) of the module.

Beside the absolute total reflectance value, the influence of the diffuse-to-specular ratio is also evaluated. The change in the diffuse-to-specular ratio of the reflective material does not have a relevant effect on the LER and the YBR (see Fig. 9), which is not that surprising. The mixing cavity erases any angular particularity of the reflection and after the first interaction with the phosphor plate, the backward scattering of yellow light becomes fully diffuse. As can be seen in Fig. 9, a more specular reflector performs slightly better, because less interactions within the mixing cavity occur. However, the effect becomes more significant when the total reflectance value is low. On the other hand, the irradiance on the phosphor plate surface oriented toward the cavity is highly influenced by the diffuse-to-specular balance in the reflective material (see Fig. 10). The irradiance non-uniformity, defined as the ratio of the difference between the maximum and minimum irradiance to the sum of both, equates 56% and 36% for a mirror-like and a perfect diffuser, respectively. The more specular, the more high density points are present, which may induce an early aging of the phosphor. Narendran *et al.* [11] have reported
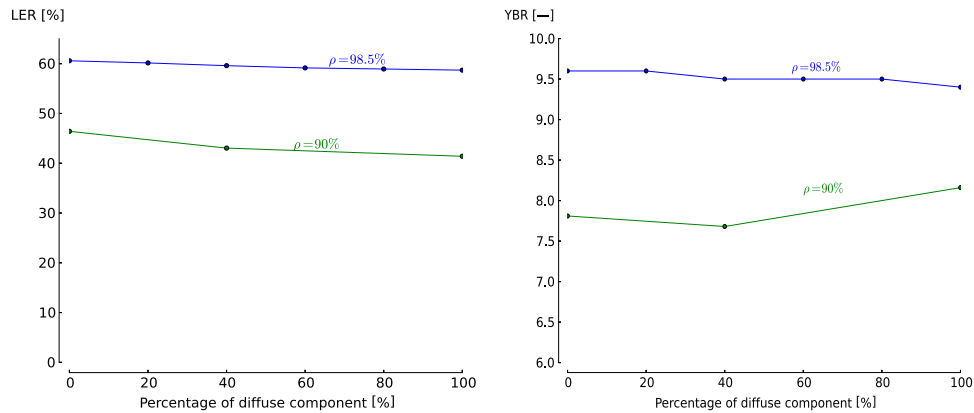
Fig. 9. LER (left) and YBR (right) for the different diffuse-to-specular ratios of the mixing cavity at two total reflectance values (height = 43 mm; LEDs intensity distribution: Lambertian).
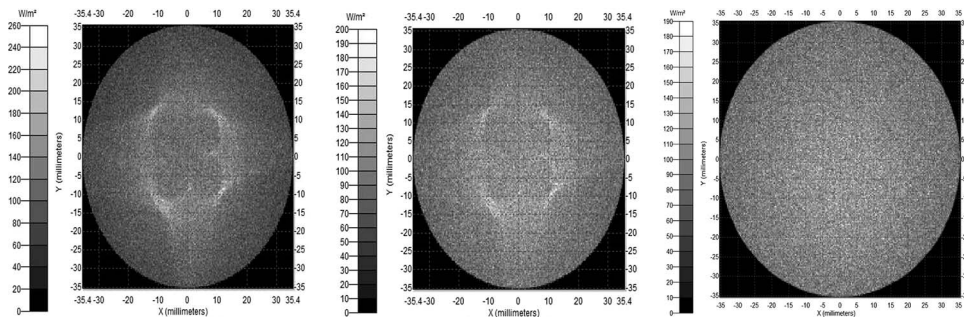

Fig. 10. Spatial irradiance on the phosphor plate (diameter = 70.8 mm, thickness = 3 mm) for the mixing cavity with: a specular reflector (left), diffuse-to-specular ratio:40% (centre), and a perfect diffuser (right).

on the negative effect that high irradiance levels have on the organic resin in which the phosphor is deposited. Although the diffuse-to-specular ratio does not influence directly the LER nor the YBR, in the long term, they could become affected as a consequence of the RPC aging.

5.3. Height of the Mixing Cavity

Another important parameter that influences the amount of light that interacts with the mixing cavity is the height-to-radius ratio of the mixing cavity. Keeping the radius at 43 mm, four different height values are considered. Simulation results in Fig. 11 show the inverse relation between the height and the LER. The smaller the height, the lower the reflection losses in the MPET due to less interactions within the cavity. Furthermore, at smaller height values more blue light reaches the RPC without interacting with the mixing cavity, as observed in Fig. 12. In turn, the average angle of incidence of the blue light for the first interaction with the RPC is smaller, increasing the blue transmission as consequence of the *bibs* characteristic illustrated in Fig. 4. However, the YBR is also influenced: the YBR is slightly lower for small cavity heights, increasing the CCT. The proximity of the RPC to the pump source affects also the irradiance and the irradiance uniformity on the RPC, bringing the irradiance non-uniformity from 36% to 91% when the height is changed from 42 mm to 10 mm (see Fig. 12). This means that there exist a clear trade-off between the LER and the irradiance uniformity. An optimum height could be selected such that the peak irradiance values stay below the critical local irradiance levels regarding thermal quenching of the phosphor film.
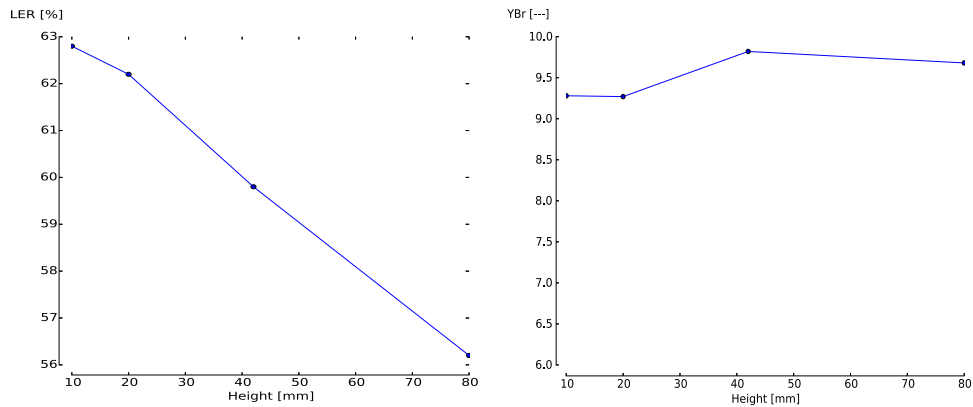
Fig. 11. LER (left) and YBR (right) for different mixing cavity height values (total reflectance:98.5%; diffuse-to-specular ratio: 98.5%; LEDs intensity distribution: Lambertian).
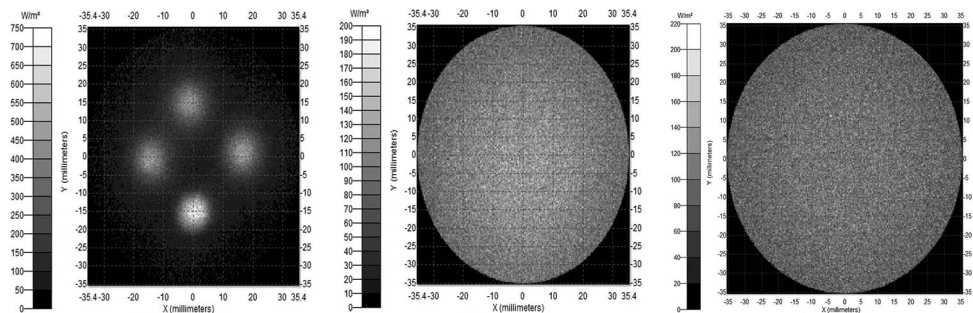

Fig. 12. Spatial irradiance on the phosphor plate when the mixing cavity has a height of 10 mm (left), 43 mm (center), and 80 mm (right).

One of the first modules applying the remote phosphor technology consisted of a cylindrical cavity with a diameter-to-height ratio of 1.5, and a diameter of 61 mm [37]. The historical evolution of this product experienced some variations in the phosphor plate and the pump LEDs, managing to improve the luminous efficacy with a factor of 2 in 5 years [37]. The portfolio of another pioneer in the niche of the remote phosphor technology [21] contained a gamut of remote phosphor products with a diameter-to-height ratio of 2.2 for a height of 10 mm. The manufacturer even continues shrinking the height with a minimum value of even 3 mm at the time this document was elaborated, making use of the positive effects on the efficacy.

5.4. Intensity Distribution of the Pump LEDs

In the previous sections, the typical Lambertian intensity distribution of the blue LEDs has been adopted. However, in Section 5.2 it was presented how the mixing cavity absorption limits the light extraction ratio from the remote phosphor module. In principle, a good alternative to minimize the losses attributed to the mixing cavity at the first hit would be to use a collimated blue beam exciting the phosphor plate. In this section the FWHM of each LED is changed between 10 degrees (collimated) and 120 degrees (Lambertian) with two values in between. The impact on the LER and YBR is given in Fig. 13.

The negligible influence of the FWHM on the LER of the module is attributed to the fact that the interaction *biys* is nearly independent on the angle of incidence (see Fig. 4, right), taking into account that the yellow contribution represents approximately the 90% of the total light extracted power. On the other hand, the dependance of the BTDF on the incident angle for the interaction
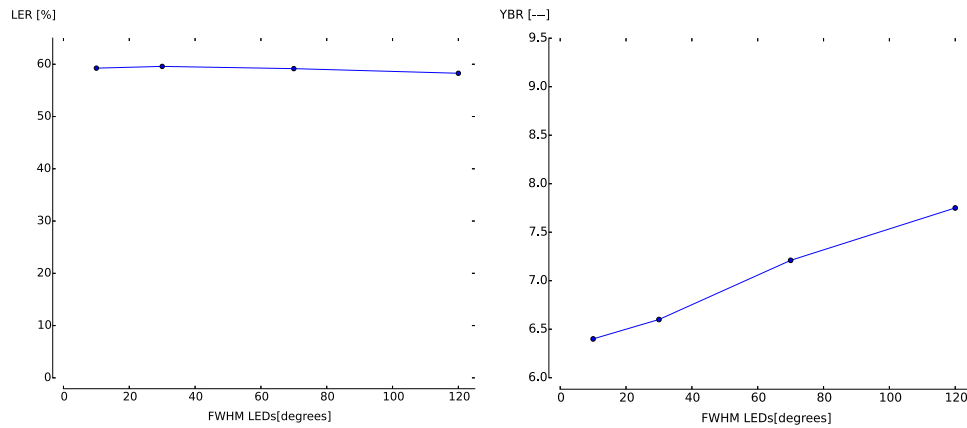
Fig. 13. Performance indicators for pump LEDs with different FWHM: LER (left), YBR (right). (Total reflectance = 98.5%; diffuse-to-specular ratio:98.5%; height = 43 mm.)
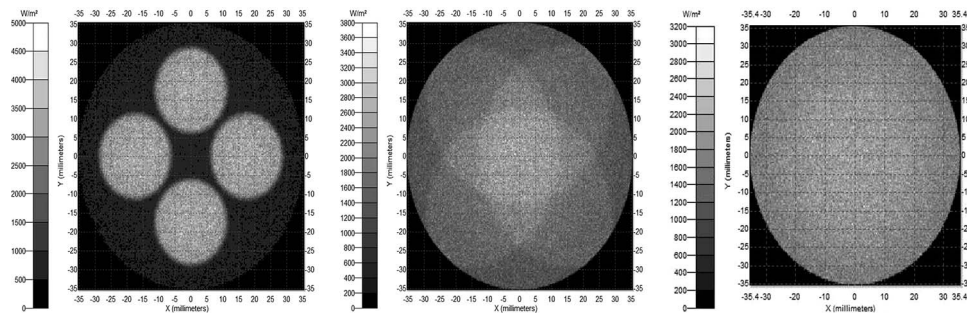

Fig. 14. Spatial irradiance on the phosphor plate for different pump LEDs' FWHM: 30° (left), 70° (center), and 120° (right).

bibs augments the extracted blue light at a small angle (see the right side of Fig. 4) which in turn has a subsequent impact on the YBR.

In addition, by using narrow beam blue LEDs a more non-uniform spatial irradiance distribution (76% for FWHM = 30°) is created on the phosphor plate (see Fig. 14), which deteriorates its reliability. Finally, the secondary optics to create the collimated beam will also introduce some losses and will increase the cost. Hence, for a cylindrical mixing cavity a Lambertian pump source remains the best option.

6. Conclusion

A simulation model applying a two-wavelength approach and considering the remote phosphor as a surface to which three BSDFs are attributed (respectively, one for the blue–blue, blue–yellow, and yellow–yellow interaction) is developed and validated. The model properly reproduces the scattering and fluorescence behavior, the total blue and yellow emitted power and the spectral radiant flux distribution.

By varying the optical and geometrical parameters of the cylindrical mixing cavity with pump LEDs on its base, the highest LER achieved was 63% using a height of 10 mm. This value slightly surpasses the maximum LER attained by an intimate pcLED (61%) [38]; however, it is still lower than the maximum LER of 68% [23] due to the losses experienced by the converted light in the mixing cavity and the transmission through the RPC. Future work should consider new topologies in which the backward scattered light can be recycled without interacting again with the phosphor plate. Only in this way, the high potential extraction ratio of the remote phosphor concept could be fully exploited.

References

[1] S. Pimputkar, J. S. Speck, S. P. Den Baars, and S. Nakamura, "Prospects for LED lighting," *Nat. Photon.*, vol. 3, no. 4, pp. 180–182, Apr. 2009.

[2] D. Hum, "Phosphor converted light source having an additional LED to provide long wavelength light," US Patent 8 395 312, Mar. 12, 2013. [Online]. Available: https://www.google.be/patents/US8395312

[3] "LED (Light-Emitting Diode) Backlight Light Source," CN Patent App. CN 201 310 269 974, Sep. 11, 2013. [Online]. Available: https://www.google.be/patents/CN103292225A?cl=en

[4] R. Mueller-Mach *et al.,* "Highly efficient all-nitride phosphor-converted white light emitting diode," *Phys. Status Solidi A*, vol. 202, no. 9, pp. 1727–1732, Jul. 2005. [Online]. Available: http://dx.doi.org/10.1002/pssa.200520045

[5] J. Y. Woo, K. Kim, S. Jeong, and C.-S. Han, "Enhanced photoluminance of layered quantum dot-phosphor nanocomposites as converting materials for light emitting diodes," *J. Phys. Chem. C*, vol. 115, no. 43, pp. 20 945–20 952, 2011.

[6] A. Keppens *et al.,* "Efficiency evaluation of phosphor-white high-power light-emitting diodes," *J. Light Vis. Environ.*, vol. 35, no. 3, pp. 199–187, Dec. 2011.

[7] N. Narendran, Y. Gu, J. P. Freyssinier, H. Yu, and L. Deng, "Solid-state lighting: Failure analysis of white LEDs," *J. Cryst. Growth*, vol. 268, no. 3/4, pp. 449–456, 2004.

[8] H.-T. Huang, Y.-P. Huang, and C.-C. Tsai, "Planar lighting system using array of blue LEDs to excite yellow remote phosphor film," *J Display Technol.*, vol. 7, no. 1, pp. 44–51, Jan. 2011.

[9] V. Bachmann, C. Ronda, and A. Meijerink, "Temperature quenching of Yellow Ce3+ Luminescence in YAG:Ce," *Chem. Mater.*, vol. 21, no. 10, pp. 2077–2084, 2009.

[10] M.-T. Lin *et al.,* "Ring remote phosphor structure for phosphor-converted white LEDs," *IEEE Photon. Technol. Lett.*, vol. 22, no. 8, pp. 574–576, Apr. 2010.

[11] Y. Zhu and N. Narendran, "Investigation of remote-phosphor white light-emitting diodes with multi-phosphor layers," *Jpn. J. Appl. Phys.*, vol. 49, no. 10, Oct. 2010, Art. ID. 100203.

[12] H.-C. Kuo *et al.,* "Patterned structure of remote phosphor for phosphor-converted white LEDs," *Opt. Exp.*, vol. 19, no. S4, pp. A930–A936, Jul. 2011.

[13] P. H. Yuen, H. H. Shiung, and M. Devarajan, "Influence of phosphor packaging configurations on the optical performance of chip on board phosphor converted warm white LEDs," in *Proc. 5th ASQED*, 2013, pp. 329–333.

[14] C. Hoelen *et al.,* "Remote phosphor LED modules for general illumination: toward 200 lm/W general lighting LED light sources," in *Proc. SPIE, 8th Int. Conf. Solid State Light.*, Aug. 2008, vol. 7058, pp. 1–10.

[15] V. Bachmann, A. Meijerink, and C. Ronda, "Luminescence properties of SrSi2AlO2N3 doped with divalent rare-earth ions," *J. Luminescence*, vol. 129, no. 11, pp. 1341–1346, Nov. 2009.

[16] S. Choi, Y. J. Yun, and H.-K. Jung, "Eu2+ and Mn2+ activated single phase white emitting phosphor Na(Sr,Ba)PO4 for phosphor converted-LEDs," *Mater. Lett.*, vol. 75, pp. 186–188, May 2012.

[17] Z. Liu, S. Liu, K. Wang, and X. Luo, "Measurement and numerical studies of optical properties of YAG:Ce phosphor for white light-emitting diode packaging," *Appl. Opt.*, vol. 49, no. 2, pp. 247–257, Jan. 2010.

[18] T. Hua, L. Ji-Wen, Q. Kun, S. Jun, and W. Da-Jian, "Color-converted remote phosphor prototype of a multiwavelength excitable borosilicate glass for white light-emitting diodes," *Chin. Phys. B*, vol. 21, no. 9, 2012, Art. ID. 098504.

[19] A. Latynina *et al.,* "Properties of Czochralski grown Ce,Gd:Y3Al5O12 single crystal for white light-emitting diode," *J. Alloys Compounds*, vol. 553, pp. 89–92, Mar. 2013.

[20] Koninklijke Philips Electronics Naamloze Vennootschap (KPENV), "Design-in guide Philips Fortimo LED downlight module (DLM)," Philips, Surrey, U.K., Oct. 2011. [Online]. Available: www.philips.com/fortimo

[21] "Product Data Sheet: XTM LED Module With Corrected Cold Phosphor Technology Vibrant Series (v80)," Xicato, San Jose, CA, USA, Dec. 2014.

[22] F. B. Leloup, S. Forment, P. Dutré, M. R. Pointer, and P. Hanselaer, "Design of an instrument for measuring the spectral bidirectional scatter distribution function," *Appl. Opt.*, vol. 47, no. 29, pp. 5454–5467, Oct. 2008.

[23] P. Acuña *et al.,* "Power and photon budget of a remote phosphor LED module," *Opt. Exp.*, vol. 22, no. S4, pp. A1079–A1092, Jun. 2014.

[24] J. E. Harvey, R. V. Shack, and J. M. Bennett, "Light-scattering characteristics of optical surfaces," Ph.D. dissertation, Arizona Univ. Tucson Opt. Sci. Center, Tucson, AZ, 1975.

[25] J. Audenaert, "Simulating luminance distributions of luminaires from ray files," Ph.D. dissertation, Arenberg Doctoral School-KU Leuven, Leuven, Belgium, Jun. 11, 2014.

[26] K. Yamada, Y. Imai, and K. Ishii, "Optical simulation of light source devices composed of blue LEDs and YAG phosphor," *J. Light Vis. Environ.*, vol. 27, no. 2, pp. 70–74, 2003.

[27] R. Hu and X. Luo, "A model for calculating the bidirectional scattering properties of phosphor layer in white light-emitting diodes," *J Lightw. Technol.*, vol. 30, no. 21, pp. 3376–3380, Nov. 2012.

[28] R. Hu *et al.,* "Study on phosphor sedimentation effect in white light-emitting diode packages by modeling multi-layer phosphors with the modified Kubelka–Munk theory," *J. Appl. Phys.*, vol. 113, no. 6, Feb. 2013, Art. ID. 063108.

[29] R. Hu, H. Zheng, J. Hu, and X. Luo, "Comprehensive study on the transmitted and reflected light through the phosphor layer in light-emitting diode packages," *J. Display Technol.*, vol. 9, no. 6, pp. 447–452, Jun. 2013.

[30] C. Sommer, P. Hartmann, P. Pachler, H. Hoschopf, and F. P. Wenzl, "White light quality of phosphor converted light-emitting diodes: A phosphor materials perspective of view," *J. Alloys Compound*, vol. 520, pp. 146–152, Apr. 15, 2012.

[31] S. Leyre *et al.,* "A hybrid tool for spectral ray tracing simulations of luminescent cascade systems," *Opt. Exp.*, vol. 22, no. 20, pp. 24 582–24 593, Oct. 2014.

[32] P. Hanselaer, A. Keppens, S. Forment, W. R. Ryckaert, and G. Deconinck, "A new integrating sphere design for spectral radiant flux determination of light-emitting diodes," *Meas. Sci. Technol.*, vol. 20, no. 9, 2009, Art. ID. 095111. [Online]. Available: http://stacks.iop.org/10.1088/0957-0233/20/9/095111

[33] R. Zheng, "Luminous efficiency and color rendering of phosphor-converted white LEDs," *J. Light Vis. Environ.*, vol. 32, no. 2, pp. 230–233, 2008.

[34] J. McKittrick and L. E. Shea-Rohwer, "Review: Down conversion materials for solid-state lighting," *J. Amer. Ceramic. Soc.*, vol. 97, no. 5, pp. 1327–1352, May 2014.

[35] S. Leyre *et al.,* "Taking the spectral overlap between excitation and emission spectra of fluorescent materials into account with Monte Carlo simulations," in *Proc. SPIE*, 2014, pp. 1–10. [Online]. Available: http://dx.doi.org/10.1117/12.2051995

[36] Y. Zhu and N. Narendran, "Optimizing the performance of remote phosphor LEDs," *J. Light Vis. Environ.*, vol. 32, no. 2, pp. 115–119, 2008.

[37] M. Oktay, "Fortimo LED DLM Flex. Webinar," Philips, Amsterdam, The Netherlands, Jun. 2014. [Online]. Available: http://www.lighting.philips.co.uk/pwc_li/main/shared/assets/images/oem/techlearning/PDF/Fortimo-LED-DLM-Flex-webinar-20th-June-2014.pdf

[38] C.-C. Sun *et al.,* "Packaging efficiency in phosphor-converted white LEDs and its impact to the limit of luminous efficacy," *J. Solid State Light*, to be published. [Online]. Available: http://dx.doi.org/10.1186/s40539-014-0019-0